
Joint Nonparametric Precision Matrix Estimation with Confounding

Sinong Geng

Princeton University

Mladen Kolar

University of Chicago

Oluwasanmi Koyejo

University of Illinois

Abstract

We consider the problem of precision matrix estimation where, due to extraneous confounding of the underlying precision matrix, the data are independent but not identically distributed. While such confounding occurs in many scientific problems, our approach is inspired by recent neuroscientific research suggesting that brain function, as measured using functional magnetic resonance imaging (fMRI), is susceptible to confounding by physiological noise such as breathing and subject motion. Following the scientific motivation, we propose a graphical model, which in turn motivates a joint nonparametric estimator. We provide theoretical guarantees for the consistency and the convergence rate of the proposed estimator. In addition, we demonstrate that the optimization of the proposed estimator can be transformed into a series of linear programming problems, and thus be efficiently solved in parallel. Empirical results are presented using simulated and real brain imaging data, which suggest that our approach improves precision matrix estimation, as compared to baselines, when confounding is present.

1 Introduction

We consider the problem of precision matrix estimation where, due to extraneous confounding of the underlying precision matrix, the data are independent but not identically distributed. While such confounding occurs in many scientific problems, our approach is inspired by applications to brain connectivity estimation from functional brain imaging. Functional brain connectivity has emerged as one of the most promising tools in the neuroscience toolbox for elucidating brain

organization [Biswal et al., 1995, Fox and Raichle, 2007] and its relationship to behavior [Sadaghiani and Kleinschmidt, 2013, Fornito et al., 2013, Zalesky et al., 2012, Barch et al., 2013]. Further, multiple studies suggest that functional brain connectivity may provide an accurate biomarker for cognitive disorders – from Alzheimer’s and schizophrenia, to autism and depression [Price et al., 2014, Arbabshirani and Calhoun, 2011], and may be key to better understanding these cognitive diseases.

However, there is growing evidence that brain function as measured using functional magnetic resonance imaging (fMRI), is susceptible to confounding by physiological noise, such as breathing and subject motion [Laumann et al., 2016, Goto et al., 2016]. In particular, these physiological signals cause complicated effects (usually non-linear), and induce incorrect strong connectivity between brain areas. Perhaps most strikingly, some authors have suggested that much of what we now think of as functional connectivity might simply reflect these physiological confounders. A variety of techniques have been proposed in the neuroimaging for addressing the effects of physiological confounders [Van Dijk et al., 2012, Power et al., 2014, Caballero-Gaudes and Reynolds, 2017], most commonly by attempting to regress out their effects from the time series, or using matrix factorization methods such as independent components analysis. While these methods may be effective for removing *linear* confounding in the observed time series (or in the covariance), none of these address our core concern of removing the effects of physiological confounding in the precision matrix, whose structure, in most of the cases, directly corresponds to the connectivity of brain areas.

In contrast to prior work, our manuscript addresses the physiological confounding via a varying statistical graphical model. Specifically, by allowing underlying models to change over each observation, the proposed method directly addresses the confounding to the precision matrices. Furthermore, we consider a novel method for precision matrix estimation from non-identically distributed data, where the extrane-

ous factors may *nonlinearly* induce additive noise in the precision matrix. Our proposed estimator is a joint nonparametric estimation (JNE) to the objective precision matrix using independent but non-identically distributed (i.n.d.) data. Surprisingly, the provided theoretical guarantees not only indicate the consistency of JNE but also point out a convergence rate comparable to that of state-of-the-art methods *without any* confounding. Also, an efficient optimization procedure based on linear programming that can easily be parallelized is applied to the parameter estimation. While the model is motivated and applied to neuroimaging, our results may be of more general interest to other applications where non-i.i.d. signals induced by confounders are prevalent, such as financial and social network applications [Lee and Hastie, 2015, Hong et al., 2012].

We summarize the main contributions of this manuscript as follows:

- We propose a graphical model for precision matrix estimation where the data are independent but not identically distributed, due to systematic effects of confounders to the underlying precision matrix.
- We propose a joint nonparametric estimator and rigorously prove its consistency and rate of convergence.
- We evaluate the resulting estimator using simulated and real brain imaging data showing improved performance when confounding is present.

The paper is organized as follows. The overall approach for graphical modeling with physiological confounder is outlined in Section 2, and our proposed joint nonparametric estimator is outlined in Section 4. Three types of models related to the proposed one are discussed in Section 3. We investigate the consistency and the convergence rate of the estimator in Section 5. Experimental results on simulated and real brain imaging data are provided in Section 6, and we conclude in Section 7.

2 Graphical Modeling of Physiological Confounders

In this section, we introduce our model for brain connectivity analysis with physiological confounders based on the framework of probabilistic graphical models. Undirected probabilistic graphical models are widely used to explore and represent dependencies among random variables [Lauritzen, 1996], in areas ranging from image processing [Mignotte et al., 2000]

to multiple testing [Liu et al., 2016] and computational biology [Friedman, 2004].

An undirected probabilistic graphical model consists of an undirected graph $\mathcal{G} = (V, E)$, where $V = \{1, \dots, p\}$ is the vertex set and $E \subset V \times V$ is the edge set, and a random vector $\mathbf{Z} = (Z_1, \dots, Z_p) \in \mathcal{Z}^p \subseteq \mathbb{R}^P$. Each coordinate of the random vector Z is associated with a vertex in V , and the graph structure encodes the conditional independence assumptions underlying the distribution of Z . In particular, Z_j and $Z_{j'}$, with $j, j' \in V$, are conditionally independent given all the other variables if and only if $(j, j') \notin E$, that is, the nodes j and j' are not adjacent in \mathcal{G} . One of the fundamental problems in statistics is that of learning the structure of \mathcal{G} from i.i.d. samples from Z and quantifying uncertainty of the estimated structure. Drton and Maathuis [2016] provides a recent review of algorithms for learning the structure of graphical models.

Gaussian graphical models are commonly used for modeling continuous \mathbf{Z} . In this case, the edge set E can be recovered by estimating the inverse covariance matrix $\mathbf{\Omega} = \mathbf{\Sigma}^{-1}$, known as the precision matrix. The sparsity pattern of the precision matrix encodes the edge set E , that is, $(j, j') \in E$ if and only if $\Omega_{jj'} \neq 0$. Therefore, sparse estimators of precision matrices, like graphical Lasso [Friedman et al., 2008] and CLIME [Cai et al., 2011], are commonly used for learning the structure of Gaussian graphical models.

We assume that we are given n independent observations $\{\mathbf{z}^i, g^i\}_{i \in [n]}$ from the joint distribution of (\mathbf{Z}, G) where $\mathbf{Z} \in \mathbb{R}^p$ is a random vector representing brain measurements and G is a random variable representing confounders, like micro-motion. Rather than assuming that the confounders only linearly affect the mean of \mathbf{Z} , as is commonly assumed in the literature [Van Dijk et al., 2012, Power et al., 2014, Caballero-Gaudes and Reynolds, 2017], we assume that the motion variable affects both the mean and the variance of \mathbf{Z} . In particular, we assume that the conditional mean $\mu(g) = \mathbb{E}(\mathbf{Z} | G = g) \in \mathbb{R}^p$ is a smooth function of the motion variable, and that the conditional covariance matrix $\mathbf{\Sigma}(g) = \text{Var}(\mathbf{Z} | G = g)$ has the inverse which takes the form

$$\mathbf{\Omega}(g) = \mathbf{\Sigma}^{-1}(g) = \mathbf{\Omega}^0 + \mathbf{R}(g). \quad (1)$$

In the above model, $\mathbf{\Omega}^0$ is the target precision matrix that we are interested in as its sparsity pattern encodes the brain connectivity, while the term $\mathbf{R}(g)$ is a nuisance component that arises due to physiological confounders such as micro-motion.

It should be noted that recovering $\mathbf{\Omega}^0$ is impossible without any constraints on $\mathbf{R}(\cdot)$. Our identifiability condition for $\mathbf{\Omega}^0$ assumes that $\mathbb{E}(\mathbf{R}(G)) = \mathbf{0}$. We jus-

tify this assumption from two perspectives. First, it is common in nonparametric estimation literature to assume that unknown curve has mean zero. Without this assumption, the constant term could be absorbed in the nonparametric component. Second, similar assumptions are confirmed by empirical studies, such as Laumann et al. [2016], where the effects of movement are shown to have minimal effects to long-term stability of brain connectivity with sufficient observations.

Furthermore, we assume that the elements of $\Sigma(g)$ are smooth functions of g , which will facilitate our nonparametric estimation procedure. Practically, in the considered micro-movement analysis area, the confounding is often assumed to be both linear and smooth [Van Dijk et al., 2012, Power et al., 2014, Caballero-Gaudes and Reynolds, 2017] like

$$\mathbb{E}[\Sigma(G) | G = g] = \beta g, \quad (2)$$

where β is the coefficient vector to be recovered by the linear regression. Therefore, we extend the linear assumption to a smooth but nonparametric assumption. We formulate these assumption rigorously in Section 5.1.

3 Related Models

The model in (1) is motivated from the perspective of multi-task learning, where for each task one has a parameter vector that can be decomposed into a common component, corresponding to Ω^0 in our setting, and a task specific component, corresponding to $\mathbf{R}(g)$ in our setting [Evgeniou and Pontil, 2004]. The goal in multi-task learning is to improve prediction performance in supervised learning, while our goal is on identifying the common brain connectivity by removing the contamination effect of motion. A big difference compared to the literature on multi-task learning is that here we have infinitely many tasks if G has a density. While in multi-task learning one may not impose additional structure on $\mathbf{R}(g)$, here we assume smoothness over the motion variable g . The effect motion can be seen through $\mathbf{R}(g)$, which modulates the strength of edges in the true structure or adds spurious edges.

Our model (1) is closely related to the literature on time-varying undirected graphical models [Zhou et al., 2010, Kolar and Xing, 2011, Yin et al., 2010, Kolar et al., 2010a,b]. However, in this literature one is interested in estimating $\Omega(g)$ as a function of time, without assuming existence of confounding effects. Simply averaging estimated $\Omega(g)$ over g for Ω^0 will lead to inefficient estimators to Ω^0 , as suggested in experiments in Section 6.1.

Another strand of the related literature focuses on estimation of multiple graphical models under the as-

sumption that they are structurally similar [Chiquet et al., 2011, Guo et al., 2011, Danaher et al., 2014, Mohan et al., 2014, Lee and Liu, 2015]. This literature is similar to multi-task learning in that the goal is to leverage similarity between multiple related graphical models, with the focus on a finite, and usually very small, number of different graphs. This class of models turn out to be not applicable to our problem as suggested in Section 6.1.

4 Joint Nonparametric Estimation to the Precision Matrix

In this section, we propose an estimator for Ω^0 under the setting described in the Section 2. Since we only have one or two observations for any $G = g$ to estimate $\Omega(g)$, we are going to pull the information from nearby observations. Specifically, we define a nonparametric estimator for the covariance matrix at $G = g$ as:

$$\mathbf{S}(g) := \frac{\sum_{i=1}^n w_i(g) \mathbf{z}^i (\mathbf{z}^i)^\top}{\sum_{i=1}^n w_i(g)} := \sum_{i=1}^n W_i(g) \mathbf{z}^i (\mathbf{z}^i)^\top, \quad (3)$$

where $w_i(g) = \psi(|g^i - g|/h)$ with a symmetric density function $\psi(\cdot)$ and $h > 0$ is a user specified bandwidth. For convenience, we define $\mathbf{S}^i := \mathbf{S}(g^i)$, $W_{i,i'} = W_i(g^{i'})$, and $\mathbf{R}^i = \mathbf{R}(g^i)$.

With the covariance matrix estimator in (3), we define the proposed JNE as

$$\begin{aligned} \hat{\Omega}^0, \{\hat{\mathbf{R}}^i\}_{i=1}^n &= \arg \min_{\mathbf{M}, \{\mathbf{R}^i\}_{i=1}^n} \left\{ \|\mathbf{M}\|_{L_1} + \frac{1}{n} \sum_{i=1}^n \|\mathbf{R}^i\|_{L_1} \right\} \\ \text{subject to } & |\mathbf{S}^i (\mathbf{M} + \mathbf{R}^i) - \mathbf{I}|_\infty \leq \lambda, \\ & i = 1, \dots, n, \\ & \sum_{i=1}^n \mathbf{R}^i = \mathbf{0}, \end{aligned} \quad (4)$$

where $|\cdot|_\infty$ denotes the elementwise L_∞ norm, $|\cdot|_1$ the L_1 vector norm, and $\|\cdot\|_{L_1}$ the L_1 matrix norm. The tuning parameter λ is user-specified and controls how close the estimated precision matrix is to the inverse of the kernel-estimated covariance matrix for each $g \in \{g^i\}$.

Notice that, similar to CLIME [Cai et al., 2011], we encourage the precision matrix to be sparse, which in our case is equivalent to a sparse M and sparse nuisance matrices \mathbf{R}^i 's. We note that recovery of Ω^0 becomes increasingly more challenging with the denseness of the nuisance matrices.

Although sharing a similar form with CLIME, JNE is special in two aspects: the sample covariance in

CLIME is replaced by local kernel estimates and the constraint incorporates all the local estimates. These two modifications allows for pooling of the information from all the samples, and as a result, JNE achieves a similar non-asymptotic sample complexity as CLIME with i.i.d. samples, as derived in Section 5.2.

Furthermore, by inheriting the form of CLIME, the objective function of JNE (4) can be decomposed by the columns of \mathbf{M} , similar to the decomposition used in Cai et al. [2011]. In particular, for a matrix \mathbf{M} , let \mathbf{M}_{*j} denote the j -th column vector. Then, for each $j = 1, \dots, p$, we consider the following p minimization problems separately:

$$\begin{aligned} & \arg \min_{\mathbf{M}_{*j}, \{\mathbf{R}_{*j}^i\}_{i=1}^n} \left\{ |\mathbf{M}_{*j}|_1 + \frac{1}{n} \sum_{i=1}^n |\mathbf{R}_{*j}^i|_1 \right\} \\ \text{subject to} & \quad |\mathbf{S}^i (\mathbf{M}_{*j} + \mathbf{R}_{*j}^i) - \mathbf{I}_{*j}|_\infty \leq \lambda, \\ & \quad i = 1, \dots, n, \\ & \quad \sum_{i=1}^n \mathbf{R}_{*j}^i = \mathbf{0}. \end{aligned} \quad (5)$$

The decomposed optimization tasks are instances of linear programs to which we apply the concurrent simplex method implemented in Gruobi [Gurobi Optimization, 2016], which solves the problems on multiple threads simultaneously. Since the solution obtained by (5) is not symmetric or positive definite in general, the final estimator is obtained after a symmetrization step similar to Cai et al. [2011].

5 Consistency of the Estimation

In this section, we establish the consistency and the non-asymptotic sample complexity of JNE under mild assumptions.

5.1 Assumptions

We start off by listing assumptions, most of which are standard in kernel-based and CLIME-based methods. Assumption 1 and 2 specify the model and the structure on the effect of confounders on the covariance of \mathbf{Z} as described in Section 2. The assumptions are going to make underlying target identifiable.

Assumption 1. We assume that random variable G has a density $f(g)$ that satisfies

$$\inf f(g) \geq C_f \geq 0 \quad \text{and} \quad |f'_k(g) - f'_k(g')| \leq C_d |g - g'|$$

for some constants C_f and C_d . The conditional distribution of \mathbf{Z} given $G = g$ is a sub-Gaussian with the variance proxy v . That is,

$$\Pr(|\mathbf{a}^\top \mathbf{Z}| > t) \leq c_1 \exp\{-c_2 \cdot v \cdot t^2\},$$

for any $\|\mathbf{a}\|_2 = 1$ and some constants c_1, c_2 .

Assumption 2. We assume that $\text{Var}(\mathbf{Z} \mid G = g) = \Sigma(g)$ with $\Omega(g) = \Sigma^{-1}(g) = \Omega^0 + \mathbf{R}(g)$ with $\mathbb{E}(\Omega(G)) = \Omega^0$.

The following assumption ensures that the local covariance matrices are well behaved. A similar related assumption was used in analysis of the CLIME procedure [Cai et al., 2011].

Assumption 3. There exist $\Lambda_\infty, C_\infty \leq \infty$ such that

$$\Lambda_\infty^{-1} \leq \inf_g \Lambda_{\min}(\Sigma(g)) \leq \sup_g \Lambda_{\max}(\Sigma(g)) \leq \Lambda_\infty,$$

and

$$\sup_g |\Sigma(g)|_\infty \leq C_\infty,$$

where $\Lambda_{\min}(\cdot)$ and $\Lambda_{\max}(\cdot)$ denote the smallest and largest eigenvalues respectively. Furthermore, there exist $C_{\mathbf{M}}, C_{\mathbf{R}} \leq \infty$ such that

$$\sup_g \|\mathbf{R}(g)\|_{L_1} \leq C_{\mathbf{R}} \quad \text{and} \quad \|\Omega\|_{L_1} \leq C_{\mathbf{M}}.$$

Since we are using a local kernel estimator, we need the following three assumptions which give regularity conditions that allow us to estimate Ω^0 . Assumption 4 imposes assumptions on the kernel function $\psi(\cdot)$ that are satisfied for a number of commonly used kernels.

Assumption 4. The kernel function $\psi(\cdot): \mathbb{R} \rightarrow \mathbb{R}$ is a symmetric probability density function supported on $[-1, 1]$. There exists a constant $C_\psi < \infty$, such that

$$\sup_x |\psi(x)| \leq C_\psi \quad \text{and} \quad \sup_x \psi(x)^2 \leq C_\psi.$$

Furthermore, $\psi(\cdot)$ is C_L -Lipschitz on $[-1, 1]$. That is

$$|\psi(x) - \psi(x')| \leq C_L |x - x'|, \quad x, x' \in [-1, 1].$$

The above assumption could be relaxed at the expense of more complicated proofs.

The next conditions assumes smoothness of the conditional mean and variance of \mathbf{Z} .

Assumption 5. There exists a constant $C_\mu < \infty$ such that

$$\sup_g \left| \frac{d}{dg} \mu(g) \right|_\infty \leq C_\mu \quad \text{and} \quad \sup_g \left| \frac{d^2}{dg^2} \mu(g) \right|_\infty \leq C_\mu.$$

Furthermore, there exists a constant $C_\Sigma < \infty$ such that

$$\sup_g \left| \frac{d}{dg} \Sigma(g) \right|_\infty \leq C_\Sigma \quad \text{and} \quad \sup_g \left| \frac{d^2}{dg^2} \Sigma(g) \right|_\infty \leq C_\Sigma.$$

| # Nodes | Mm-CLIE | Ke-CLIME | Re-CLIME |
|---------|---------|----------|----------|
| 10 | 0.078 | 0.078 | 0.039 |
| 15 | 0.117 | 0.078 | 0.117 |
| 20 | 0.117 | 0.117 | 0.117 |
| 25 | 0.117 | 0.156 | 0.156 |

Table 1: Summary of the regularization parameters used for the considered methods using the synthetic datasets.

Although complicated, the proposed assumptions are designed to relax the existing linear assumption (2) widely used in the neuroimaging literature [Van Dijk et al., 2012, Power et al., 2014, Caballero-Gaudes and Reynolds, 2017]. Also, such assumptions are commonly used in nonparametric works to relax a parametric assumption.

With the assumptions, we are ready to present our main result in the next section.

5.2 Convergence rate of $\hat{\Omega}^0$

Now, we provide the consistency and the non-asymptotic sample complexity of $\hat{\Omega}^0$ by Theorem 1.

Theorem 1. Suppose that the assumptions mentioned in Sections 5.1 are satisfied. Given n independent observations $\{\mathbf{z}^i, g^i\}_{i \in [n]}$, we assume that there are $C_1 > 0$ and $C_2 > 0$, satisfying

$$\min_{\{j, j' \mid \exists i \in [n], \Omega_{jj'}(g^i) \neq 0\}} \sqrt{n^{-1} \sum_{i \in [n]} (\Omega_{jj'}(g^i))^2} \leq C_1 \sqrt{\log pn}^{-2/5},$$

where

$$n \geq C_2 d^{5/2} (\log p)^{5/4},$$

and

$$\lambda = \frac{(C_M + C_R)}{C_2} \sqrt{(r+1) \log p - \log C_1} n^{-2/5}.$$

d denotes the maximum node degree of the graph.

Then, for any $r > 0$, we have

$$\begin{aligned} & \left| \hat{\Omega}^0 - \Omega^0 \right|_{\infty} \\ & \leq \frac{3(C_M + C_R)^2}{C_2} \sqrt{(r+1) \log p - \log C_1} n^{-2/5} \quad (6) \\ & \quad + \frac{C_M}{\sqrt{2}} \sqrt{(r+2) \log p + \log 2} n^{-1/2}, \end{aligned}$$

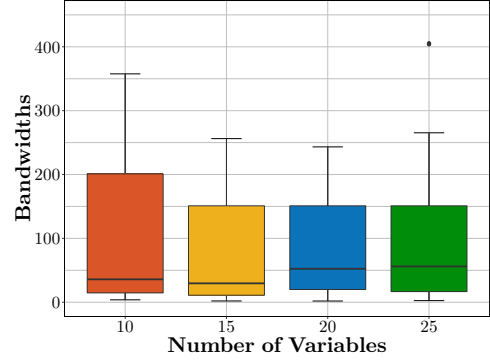


Figure 1: Bandwidths for models with different numbers of variables for the synthetic datasets.

with probability larger than $1 - 2p^{-r}$.

In words, Theorem 1 indicates that, with a high probability, the estimation error is bounded by $O\left(\sqrt{\frac{\log p}{n^{4/5}}}\right)$.

Inevitably, it is slightly larger than $O\left(\sqrt{\frac{\log p}{n}}\right)$, i.e., the non-asymptotic sample complexity of CLIME with n i.i.d. data. Therefore, even in the presence of confounding, we can consistently and efficiently estimate the underlying precision matrix Ω^0 that encodes true connectivity pattern, with a convergence rate comparable to CLIME without any confounding.

5.3 Proof Sketch

We provide a rough sketch idea on the proof for Theorem 1, and defer the details to the Supplements.

To begin with, we need the following Lemma 1 on the convergence of $\mathbf{S}(g)$ to $\Sigma(g)$, since the derived estimator $\hat{\Omega}^0$ is highly dependent on the nonparametric estimator $\mathbf{S}(g)$.

Lemma 1. Suppose that the Assumption 1 and Assumption 3 to 5 in Section 5.1 are satisfied, and that C_1 and C_2 are defined in Theorem 1. Then, for any $r > 0$,

$$\Pr\left\{\sup_g |\mathbf{S}(g) - \Sigma(g)|_{\infty} \geq \lambda\right\} \leq p^{-r}, \quad (7)$$

where $\lambda = \frac{\sqrt{(r+1) \log p - \log C_1}}{C_2} n^{-2/5}$.

Lemma 1 provides a uniform convergence result over g of the local covariance estimator.

Then, instead of directly studying $\left|\hat{\Omega}^0 - \Omega^0\right|_{\infty}$, we start by bounding $\left|\hat{\Omega}^0 - \mathbf{M}\right|_{\infty}$, where $\mathbf{M} = \frac{\sum_{i \in [n]} \Omega(g^i)}{n}$. Specifically, with Lemma 1, we derive Lemma 2 on the relationship between $\hat{\Omega}^0$ and \mathbf{M} .

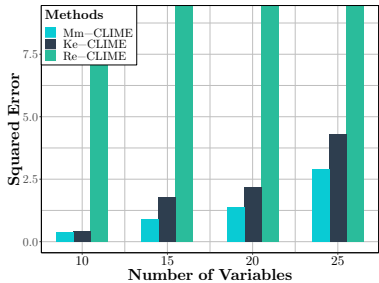


Figure 2: Squared error for the considered methods with the selected λ 's using synthetic datasets.

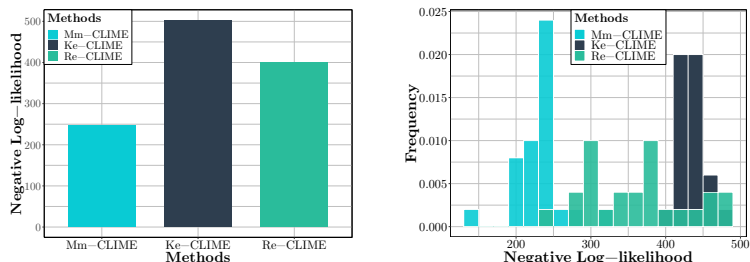


Figure 3: Barplot of estimated negative log-likelihoods using the selected λ 's, histogram of the considered methods with all λ 's, using the COBRE dataset.

Lemma 2. Suppose that the conditions in Theorem 1 are satisfied. Then, for any $r > 0$,

$$\begin{aligned} & \left| \hat{\Omega}^0 - \mathbf{M} \right|_{\infty} \\ & \leq \frac{3(C_{\mathbf{M}} + C_{\mathbf{R}})^2}{C_2} \sqrt{(r+1) \log p - \log C_1} n^{-2/5}, \end{aligned} \quad (8)$$

with probability larger than $1 - p^{-r}$, where $\mathbf{M} = \frac{\sum_{i \in [n]} \Omega(g^i)}{n}$.

Finally, we bound $|\mathbf{M} - \Omega^0|_{\infty}$ by a union bound and the Hoeffding inequality, and thus prove Theorem 1.

6 Experiments

In what follows, we will demonstrate that the proposed method efficiently recovers the target precision matrix when applied to synthetic data in Section 6.1. Then, to illustrate that the proposed model is readily applicable to practical analysis of brain connectivity, we apply it to a resting-state functional magnetic resonance imaging dataset collected for the study on schizophrenia [Bellec].

6.1 Synthetic Experiments

In this section, we compare the proposed model with some existing models using synthetic data. Specifically, we consider a generative model where the underlying precision matrix varies smoothly with respect to the confounder variable G . Then, we generate samples with varying precision matrices via the following procedure:

1. We set the length of the multivariate random variable \mathbf{Z} to $p = 10, 15, 20, 25$, and implement the following steps separately.

2. We randomly generate 11 precision matrices as anchors, denoted by $\Omega^1, \Omega^{11}, \dots, \Omega^{101}$. Specifically, each element of the anchor precision matrices is drawn randomly to be non-zero with probability 0.2. The values of non-zero elements follow a uniform distribution.
3. Precision matrices between every two consecutive anchor precision matrices are simulated by linear interpolation.
4. For each precision matrix, we generate 2 independent zero-mean multivariate Gaussian samples, which constitute the synthetic dataset, \mathbb{Z} .
5. We set the target precision matrix as $\Omega^0 = \frac{\sum_{i=1}^{101} \Omega^i}{101}$. The considered methods are applied to \mathbb{Z} to estimate Ω^0 .

Note that by following the procedure above, the simulated model is equivalent to a generative model with fixed precision Ω^0 and additive confounding $\mathbf{R}^i = \Omega^0 - \Omega^i$, where the superscripts indicate the confounder variable G .

The proposed method is a CLIME-based movement modeling method, and thus is denoted by Mm-CLIME. According to the analysis in Section 2, the competing methods fall into three categories: the precision matrix estimation with confounding (which is designed exactly for our problem setting), time-varying precision matrix estimation [Zhou et al., 2010, Kolar and Xing, 2011, Yin et al., 2010, Kolar et al., 2010a,b], and multiple precision matrix estimation [Chiquet et al., 2011, Guo et al., 2011, Danaher et al., 2014, Mohan et al., 2014, Lee and Liu, 2015]. For the reason to be discussed later, we study two benchmarks: Re-CLIME and Ke-CLIME from the first two categories.

The baseline Re-CLIME refers to the procedure that linearly regresses out the confounding by G from the

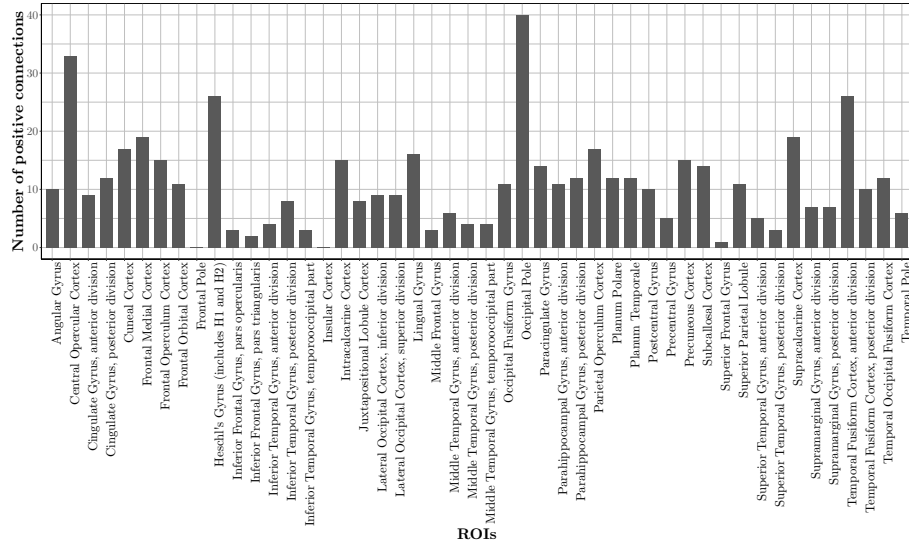


Figure 4: Number of positive connections across ROIs of the subjects diagnosed with schizophrenia recovered by the proposed method.

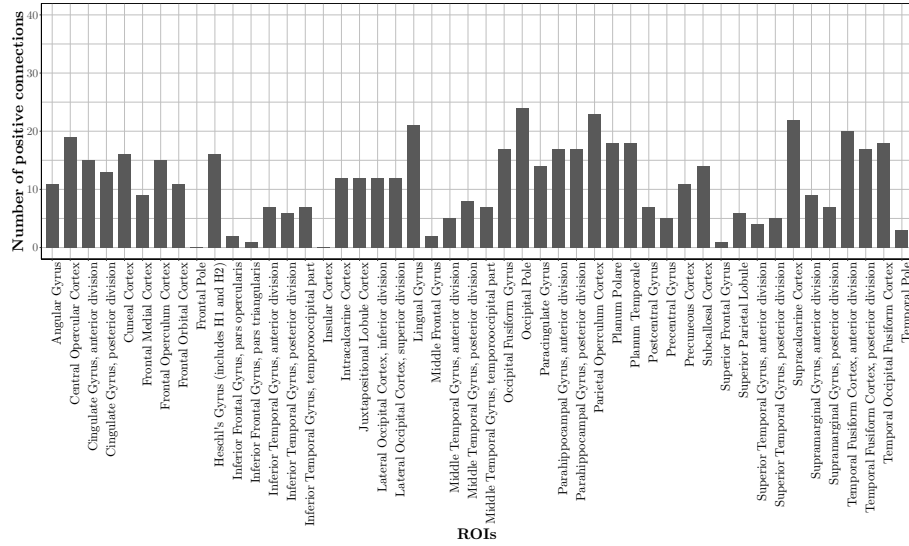


Figure 5: Number of positive connections across ROIs of the control subjects recovered by the proposed method.

observed samples first, and then uses CLIME to estimate the precision matrix. As a precision matrix estimation method with confounding, Re-CLIME is widely applied to brain functional connectivity analysis in practice [Van Dijk et al., 2012, Power et al., 2014]. Furthermore, we consider the Ke-CLIME a CLIME version of the method studied in [Kolar and Xing, 2011] as a representative of time-varying precision matrix estimation. In this case, CLIME is separately applied to kernel estimators of the covariance matrix at each observation, which results in 101 estimated precision matrices i.e estimates if the to time-varying precision matrices. We use the average of the precision matrices as an estimator of Ω^0 .

We chose to focus on CLIME-based estimators exclusively. Otherwise, whether the efficiency gain of JNE comes from the joint estimation or CLIME will be unclear. In particular, we did not evaluate the method in [Kolar and Xing, 2011], which combines kernel estimation with Graphical Lasso [Friedman et al., 2008].

Multiple precision matrix estimation methods are not included due to numerical issues. We observe that such methods require sufficient samples for the estimation of each precision matrix. Empirical evaluation of one such approach Lee and Liu [2015] most often resulted in ill-defined optimization problems without optimal solutions, since we may have as few as two observations for each precision matrix.

To strike a fair comparison, we only select CLIME-based methods from each category. The solutions obtained by considered methods are not guaranteed to be symmetric or positive definite in general. To deal with this, a procedure provided in Cai et al. [2011] is used to symmetrize solution of each method.

The Epanechnikov kernel is used with the bandwidth parameters selected by leave-one-out cross-validation. Since all the considered kernel-based methods use the same estimator of the covariance matrix, the same bandwidth are used across all the methods. Different bandwidths are used to estimate each component of the covariance matrix, resulting in $p(p-1)/2$ bandwidths. Values of these bandwidths are provided in Figure 1. The regularization parameters (λ 's) are determined by the Akaike information criterion (AIC). The selected λ 's are reported in Table 1.

The results are summarized in Figure 2. Notice that the proposed Mm-CLIME achieves the smallest squared error among all the considered methods. Furthermore, although Re-CLIME is widely used in practice to analyze the brain connectivity, it performs worst in terms of accuracy in our experiments. Actually, this is not surprising, since the effects of confounders on the observed data are seldom linear, both in our synthetic setting and practical problems.

6.2 fMRI Experiments

Functional brain connectivity measures associations between brain areas, and are thought to reflect communication and coordination between spatially distant neural populations – corresponding to information processing pathways in the brain. There are a wide variety of techniques for estimating functional connectivity in the literature [Sadaghiani and Kleinschmidt, 2013, Fornito et al., 2013, Zalesky et al., 2012, Barch et al., 2013], most commonly via the correlation. However, there is increasing evidence that the precision matrix results in a more stable and effective connectivity estimate than the alternatives [Varoquaux et al., 2010, Poldrack et al., 2015]. For this reason, we focus our attention on precision matrix estimation. We also focus on motion confounding – one of the most pressing examples of physiological confounding in the literature.

Our experiments use previously collected data [Bellec], from the Center for Biomedical Research Excellence¹ (COBRE) [COB]. We compare the considered methods using preprocessed resting-state functional magnetic resonance images for 70 patients diagnosed with schizophrenia, and 72 healthy controls. Every patient

¹We defer to the dataset authors for additional pre-processing details.

has more than 150 fMRI observations each with 22 corresponding confounders. We use the 7 confounders provided in the dataset related to motion for the analysis. Furthermore, we apply Harvard-Oxford Atlas to generate 48 atlas regions of interest (ROIs).

To start with, we quantitatively compared the performances of the methods by analyzing the held out log-likelihood of the COBRE dataset. A glass brain figure illustrating the achieved precision estimation can be found in the Supplements. Our hypothesis is that the confounding has a similar effect as additive noise. Thus, better estimation of the average precision will correspond to higher likelihood. The results using the λ selected by AIC and the results using all considered λ 's are both summarized in Figure 3. As expected, we find that the proposed method achieves the highest log-likelihood on the held-out dataset, which suggests that it results in a better model of the brain connectivity than the baselines.

Next, we apply the proposed method to the subjects diagnosed with schizophrenia and the healthy controls separately. The results are summarized in Figure 4 and Figure 5, where the number of positive connections for each ROI are reported. We notice that the connectivity of the ROIs of the subjects with schizophrenia are similar to that of the control group, except the Occipital Pole and Central Opercular Cortex have abnormally more positive connections with other ROIs, i.e., most highly connected areas. Interestingly, these two areas have been implicated in the literature as highly associated with schizophrenia [Sheffield et al., 2015, Tohid et al., 2015]. In summary, the proposed method models the fMRI accurately, and detects the differences between the subjects with schizophrenia and the control group.

7 Conclusion

We developed a novel approach for precision matrix estimation where, due to extraneous confounding of the underlying precision matrix, the data are independent but not identically distributed. For this, we proposed a varying graphical model, and an associated joint nonparametric estimator. Our technical contributions included theoretical consistency and convergence rate guarantees for the proposed estimator, and an efficient optimization procedure. Empirical results were also presented using simulated and real brain imaging data, which suggests that our approach improves precision matrix estimation as compared to a variety of baselines. For future work, we plan to investigate more complex hierarchical graphical models including more confounder effects, and joint estimation across groups to better estimate shared global structure.

References

- Cobre. http://fcon_1000.projects.nitrc.org/indi/retro/cobre.html. (Accessed on 05/12/2018).
- M. R. Arbabshirani and V. D. Calhoun. Functional network connectivity during rest and task: comparison of healthy controls and schizophrenic patients. In *Engineering in Medicine and Biology Society, EMBC, 2011 Annual International Conference of the IEEE*, pages 4418–4421. IEEE, 2011.
- D. M. Barch, G. C. Burgess, M. P. Harms, S. E. Petersen, B. L. Schlaggar, M. Corbetta, M. F. Glasser, S. Curtiss, S. Dixit, C. Feldt, et al. Function in the human connectome: task-fMRI and individual differences in behavior. *Neuroimage*, 80:169–189, 2013.
- P. Bellec. Projects/cobre at master · simexp/projects · GitHub. <https://github.com/SIMEXP/Projects/tree/master/cobre>. (Accessed on 05/12/2018).
- B. Biswal, F. Zerrin Yetkin, V. M. Haughton, and J. S. Hyde. Functional connectivity in the motor cortex of resting human brain using echo-planar MRI. *Magnetic resonance in medicine*, 34(4):537–541, 1995.
- C. Caballero-Gaudes and R. C. Reynolds. Methods for cleaning the bold fMRI signal. *Neuroimage*, 154:128–149, 2017.
- T. T. Cai, W. Liu, and X. Luo. A constrained ℓ_1 minimization approach to sparse precision matrix estimation. *J. Am. Stat. Assoc.*, 106(494):594–607, 2011.
- J. Chiquet, Y. Grandvalet, and C. Ambroise. Inferring multiple graphical structures. *Stat. Comput.*, 21(4):537–553, 2011.
- P. Danaher, P. Wang, and D. M. Witten. The joint graphical lasso for inverse covariance estimation across multiple classes. *J. R. Stat. Soc. B*, 76(2):373–397, Mar 2014. doi: 10.1111/rssb.12033. URL <http://dx.doi.org/10.1111/rssb.12033>.
- M. Drton and M. H. Maathuis. Structure learning in graphical modeling. *To appear in Annual Review of Statistics and Its Application*, 3, 2016.
- T. Evgeniou and M. Pontil. Regularized multi-task learning. In *Proceedings of the tenth ACM SIGKDD international conference on Knowledge discovery and data mining*, pages 109–117. ACM, 2004.
- A. Fornito, A. Z. Lee, and M. Breakspear. Graph analysis of the human connectome: Promise, progress, and pitfalls. *NeuroImage*, 80:426–444, 2013.
- M. D. Fox and M. E. Raichle. Spontaneous fluctuations in brain activity observed with functional magnetic resonance imaging. *Nature Reviews Neuroscience*, 8(9):700–711, 2007.
- J. Friedman, T. Hastie, and R. Tibshirani. Sparse inverse covariance estimation with the graphical lasso. *Biostatistics*, 9(3):432–441, 2008.
- N. Friedman. Inferring cellular networks using probabilistic graphical models. *Science*, 303(5659):799–805, 2004.
- M. Goto, O. Abe, T. Miyati, H. Yamasue, T. Gomi, and T. Takeda. Head motion and correction methods in resting-state functional MRI. *Magnetic Resonance in Medical Sciences*, 15(2):178–186, 2016.
- J. Guo, E. Levina, G. Michailidis, and J. Zhu. Joint estimation of multiple graphical models. *Biometrika*, 98(1):1–15, 2011.
- I. Gurobi Optimization. Gurobi optimizer reference manual, 2016. URL <http://www.gurobi.com>.
- L. Hong, A. Ahmed, S. Gurumurthy, A. J. Smola, and K. Tsioutsoulouklis. Discovering geographical topics in the twitter stream. In *Proceedings of the 21st international conference on World Wide Web*, pages 769–778. ACM, 2012.
- M. Kolar and E. P. Xing. On time varying undirected graphs. In *Proc. of AISTATS*, 2011.
- M. Kolar, A. P. Parikh, and E. P. Xing. On sparse nonparametric conditional covariance selection. In J. Fürnkranz and T. Joachims, editors, *Proc. 27th Int. Conf. Mach. Learn.*, Haifa, Israel, 2010a.
- M. Kolar, L. Song, A. Ahmed, and E. P. Xing. Estimating Time-varying networks. *Ann. Appl. Stat.*, 4(1):94–123, 2010b.
- T. O. Laumann, A. Z. Snyder, A. Mitra, E. M. Gordon, C. Gratton, B. Adeyemo, A. W. Gilmore, S. M. Nelson, J. J. Berg, D. J. Greene, et al. On the stability of bold fMRI correlations. *Cerebral cortex*, 27(10):4719–4732, 2016.
- S. L. Lauritzen. *Graphical Models*, volume 17 of *Oxford Statistical Science Series*. The Clarendon Press Oxford University Press, New York, 1996. ISBN 0-19-852219-3. Oxford Science Publications.
- J. D. Lee and T. J. Hastie. Learning the structure of mixed graphical models. *Journal of Computational and Graphical Statistics*, 24(1):230–253, 2015.
- W. Lee and Y. Liu. Joint estimation of multiple precision matrices with common structures. *Journal of Machine Learning Research*, 16:1035–1062, 2015. URL <http://jmlr.org/papers/v16/lee15a.html>.
- J. Liu, C. Zhang, D. Page, et al. Multiple testing under dependence via graphical models. *The Annals of Applied Statistics*, 10(3):1699–1724, 2016.
- M. Mignotte, C. Collet, P. Perez, and P. Bouthemy. Sonar image segmentation using an unsupervised hi-

- erarchical mrf model. *IEEE transactions on image processing*, 9(7):1216–1231, 2000.
- K. Mohan, P. London, M. Fazel, D. M. Witten, and S.-I. Lee. Node-based learning of multiple gaussian graphical models. *J. Mach. Learn. Res.*, 15:445–488, 2014. URL <http://arxiv.org/abs/1303.5145>.
- R. A. Poldrack, T. O. Laumann, O. Koyejo, B. Gregory, A. Hover, M.-Y. Chen, K. J. Gorgolewski, J. Luci, S. J. Joo, R. L. Boyd, et al. Long-term neural and physiological phenotyping of a single human. *Nature communications*, 6:8885, 2015.
- J. D. Power, A. Mitra, T. O. Laumann, A. Z. Snyder, B. L. Schlaggar, and S. E. Petersen. Methods to detect, characterize, and remove motion artifact in resting state fmri. *Neuroimage*, 84:320–341, 2014.
- T. Price, C.-Y. Wee, W. Gao, and D. Shen. Multiple-network classification of childhood autism using functional connectivity dynamics. In *International Conference on Medical Image Computing and Computer-Assisted Intervention*, pages 177–184. Springer, 2014.
- S. Sadaghiani and A. Kleinschmidt. Functional interactions between intrinsic brain activity and behavior. *Neuroimage*, 80:379–386, 2013.
- J. M. Sheffield, G. Repovs, M. P. Harms, C. S. Carter, J. M. Gold, A. W. MacDonald III, J. D. Ragland, S. M. Silverstein, D. Godwin, and D. M. Barch. Fronto-parietal and cingulo-opercular network integrity and cognition in health and schizophrenia. *Neuropsychologia*, 73:82–93, 2015.
- H. Tohid, M. Faizan, and U. Faizan. Alterations of the occipital lobe in schizophrenia. *Neurosciences*, 20(3):213, 2015.
- K. R. Van Dijk, M. R. Sabuncu, and R. L. Buckner. The influence of head motion on intrinsic functional connectivity mri. *Neuroimage*, 59(1):431–438, 2012.
- G. Varoquaux, A. Gramfort, J.-B. Poline, and B. Thirion. Brain covariance selection: Better individual functional connectivity models using population prior. In J. D. Lafferty, C. K. I. Williams, J. Shawe-Taylor, R. S. Zemel, and A. Culotta, editors, *Proc. of NIPS*, pages 2334–2342, 2010.
- J. Yin, Z. Geng, R. Li, and H. Wang. Nonparametric covariance model. *Stat. Sinica*, 20:469–479, 2010.
- A. Zalesky, A. Fornito, and E. Bullmore. On the use of correlation as a measure of network connectivity. *Neuroimage*, 60(4):2096–2106, 2012.
- S. Zhou, J. D. Lafferty, and L. A. Wasserman. Time varying undirected graphs. *Mach. Learn.*, 80(2-3): 295–319, 2010.